PNAS

Supporting Information for

Multiplexing of Cognitive Encoding by Oculomotor Networks Leads to Incidental Gaze Shifts

Matthew C. Rosen and David J. Freedman

Corresponding authors: Matthew C. Rosen, David J. Freedman
Email: matthew.casciola.rosen@gmail.com, dfreedman@uchicago.edu

This PDF file includes:

Supporting text
Figures S1 to S7
Tables S1 to S2

Supporting Information Text

Materials and Methods

Pseudo-population decoding of gaze shift direction: To capture how informative neuronal population activity in SC is about the direction of an upcoming gaze shift (SI Appendix Figure S6), we used a pseudo-population decoding approach (24). Pseudo-populations of SC units spanning separate recording days were assembled as follows. For each unit, spike trains were aligned to the onset of gaze shifts during the initial fixation period at the beginning of each trial, smoothed (Gaussian filter, width=5ms), downsampled (resolution=5ms), and labeled with the hemifield into which the corresponding shift moved gaze (left/right). These single-unit, single-shift responses were combined to form a pseudo-population response: for each shift direction/recorded unit, K single-trial responses were sampled independently at random (with replacement) and concatenated to generate an K x T x N response matrix (K pseudo-trials, T timepoints, N units). Linear SVM classifiers were fit to classify shift direction from the N-dimensional responses in the 50ms window centered on gaze-shift onset. We used K = 200 pseudo-trials (100 for shifts directed toward the left hemifield and 100 for shifts directed toward the right), but obtained similar results for other choices of K.

To allow for cross-validated classification of shift direction, this procedure was adapted to generate separate pseudo-populations for training/testing: each unit's single-shift responses were first partitioned in half, for each shift direction, before random sampling/concatenation. This ensured that classifiers were trained and tested on completely non-overlapping spike trains. To capture variability across neurons/gaze shifts, we repeated this procedure 1000 times for each animal.

Distinguishing between trials with the most- and least-prominent category-correlated eye movements: To probe the relationship between category-correlated eye movements and category-correlated neural activity in SC and LIP, we evaluated the strength of category encoding on trials with the most and least prominent category-correlated eye movements (SI Appendix Fig. S4). Within each session, after down-sampling eye position records on each trial (resolution=50ms), the prominence of category-correlated eye movements was assessed as follows: at each timepoint *t* from sample onset to test onset, we computed average eye positions for each category, taking the difference between them to obtain d_t, the direction in gaze-space along which eye positions are maximally separated by category. The sum of each trial's eye position timecourse projected onto these d_t yields a signed score that captures how closely eye movements on that trial track the average eye position for either category relative to the other through time. Scores closer to 0 indicate less consistent differentiation of eye positions by category, while scores with larger magnitude indicate more differentiation of the eye trace along d_t. The sign of the score on any trial indicates which category's average eye position trace most closely matched eye positions on that trial (positive for one category, negative for the other).

We used these scores to split trials in each session into 2 groups for each sample motion direction – the half of trials with eye movements that most vs. least closely match the average eye movement trace for the corresponding sample category. We then used these 2 groups of trials for each session/recorded neuron to build 2 separate pseudo-populations, as described in "Pseudo-population decoding of gaze shift direction", for each dataset – one using the trials with the most prominent category-correlated eye movements, the other using the trials with the least prominent category-correlated eye movements. We used the average delay period activity (from 250ms after sample offset until the time of test onset) in these pseudo-populations to decode sample category.

Quantifying impacts of muscimol inactivation on eye movements: To assess the impact of SC/LIP inactivation on fixational eye movements, we evaluated the distribution of eye position displacements in the initial DMC fixation period during inactivation vs. control conditions. We began by assembling eye positions on all DMC trials in which a sample stimulus was presented (e.g. only excluding trials terminated due to very early breaks in fixation). From this set of eye

positions, we computed the displacement between samples at each successive 50ms step – e.g. displacement in d.v.a. between eye positions sampled at 0ms and 50ms, 50ms and 100ms, etc. We chose 50ms as the step size because it is large enough to avoid being overly sensitive to high-frequency noise in the eye tracking, but small enough to allow sufficient samples for estimating displacement distributions for control/inactivation conditions. This procedure yielded two distributions of eye displacements for each animal – one during inactivation conditions, the other during control conditions. During SC inactivation experiments, where control and inactivation behavior were assessed within the same session (each session began with a period of control behavior before muscimol infusion), we assessed the significance of the difference between these distributions during each session of behavior using a 2-sample Epps-Singleton test. P-values were adjusted to control for false discovery rate across multiple sessions using the Benjamini-Hochberg procedure. For LIP inactivation data, during which control behavior was assessed in separate behavioral sessions, we aggregated displacement distributions across all control sessions and all inactivation sessions for each animal before testing for significance.

Figures

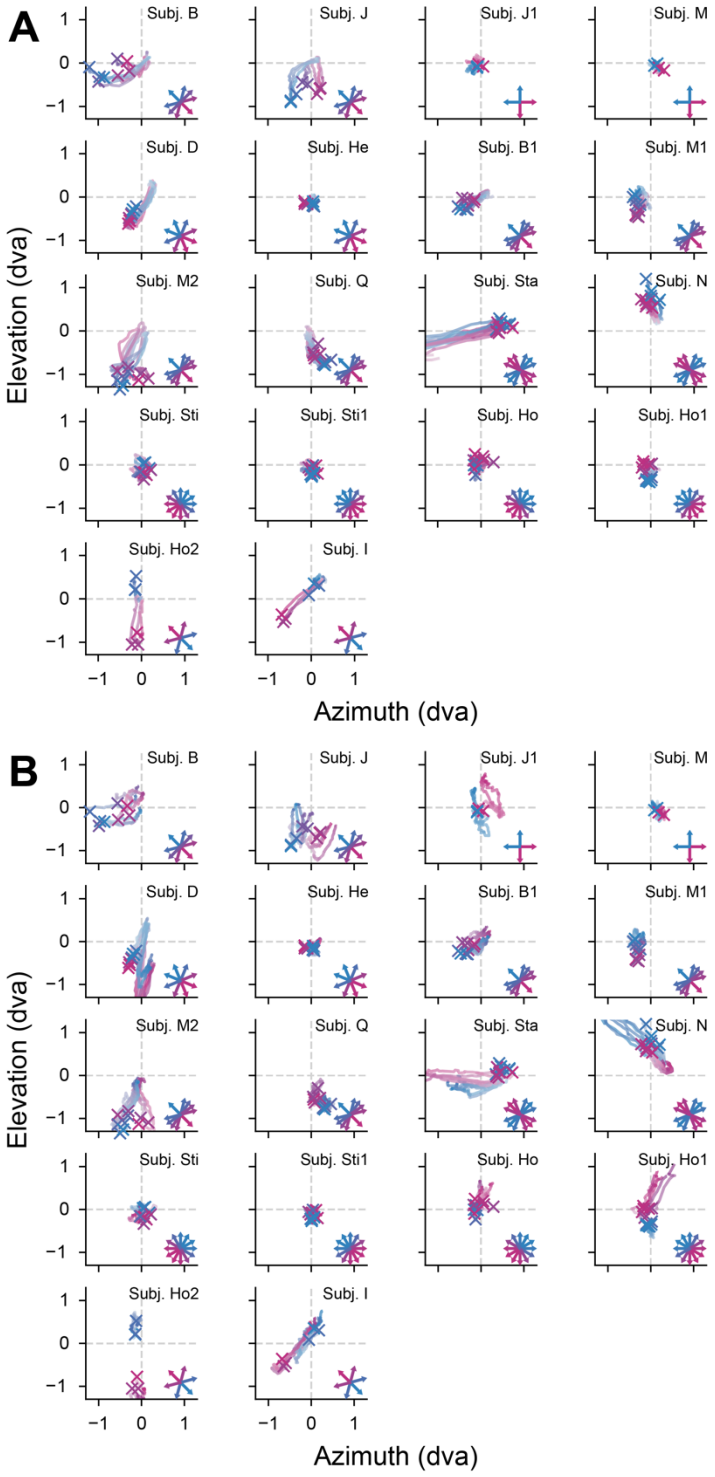

Figure S1: Gaze patterns by category for each subject/dataset. A. Gaze patterns (one trace per motion direction, averaged across trials in one example session) from fixation onset through the end of the sample period, marked with an X. Inset axis shows motion directions used for each

experiment, colored by category. Each panel shows data from a different dataset; panels are grouped by experiment. **B**. Same as in **A**, but during the delay period (X marks the beginning of the delay).

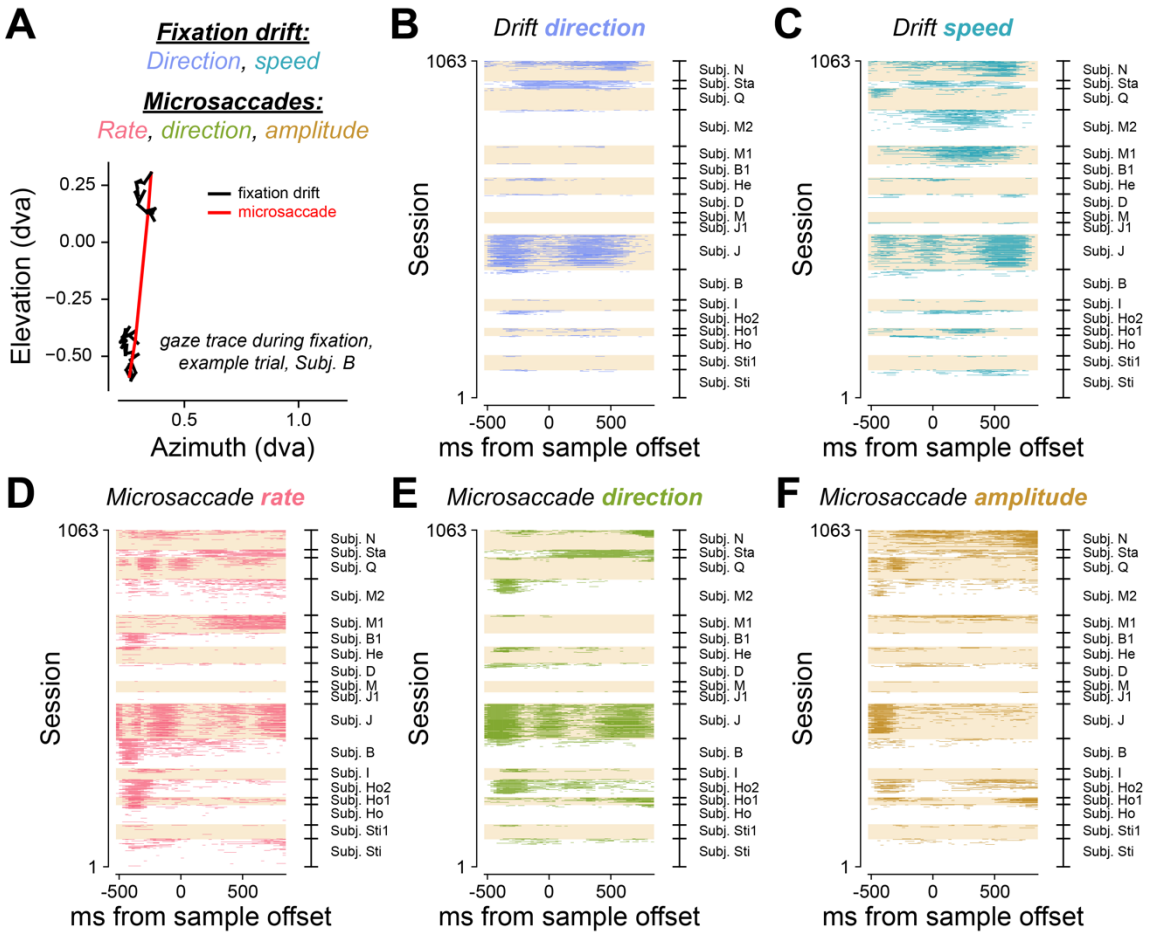

Figure S2: Between-category differences in the features of fixational drift and microsaccades. A. Bottom: Example eye position trace during fixation for one animal, with fixational drift shown in black and a microsaccade shown in red. Top: breakdown of the eye movement features evaluated. **B-F**. Heatmap showing when during each session (each row) a given feature of eye movements differed significantly between categories ($P < 0.05$, FDR-corrected through time for each session). For shift rate, P-values were obtained using a bootstrap test; for drift speed and microsaccade amplitude, a Mann-Whitney U test; and for drift/microsaccade direction, Watson's U^2 test for circular data. **B/C**: significance maps for drift direction/speed; **D/E/F:** significance maps for microsaccade rate/direction/amplitude.

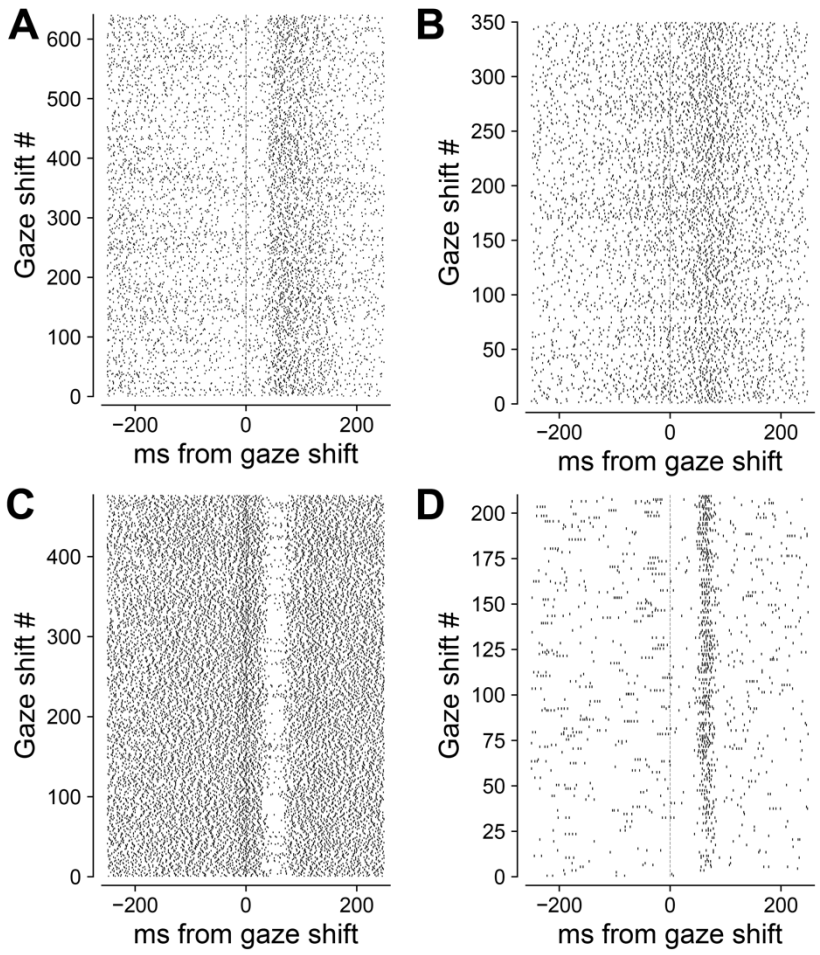

Figure S3: Significant responses after gaze shifts in LIP and SC. A-B. Raster plots of responses aligned to gaze shifts during the DMC delay period, 2 example LIP neurons. **C-D**. Raster plots of responses aligned to gaze shifts during the DMC delay period, 2 example SC neurons.

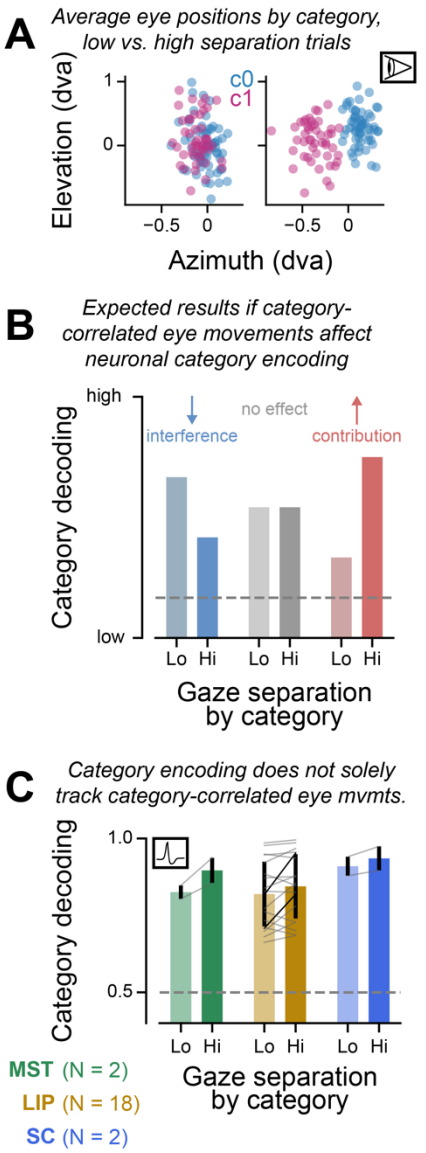

Figure S4: Category-correlated eye movements do not affect category encoding in LIP and SC. **A**. Average eye movements on trials with the least (left) vs. most (right) separation by category, 1 example session, Monkey B. Each dot denotes eye position averaged through time on one trial, colored by category. **B**. Graphic schematizing predicted patterns of category decoding in the trials with the least vs. most separation in eye movements by category. **C**. Decoding of category during the delay period from trials with low vs. high category-correlated separation in eye movements (mean +/-SEM across datasets; MST: 2 datasets; SC: N = 2 datasets; LIP: N = 18 datasets). Individual lines show data for individual datasets; black lines show datasets where the difference in decoding was significant (bootstrap test, $P < 0.05$).

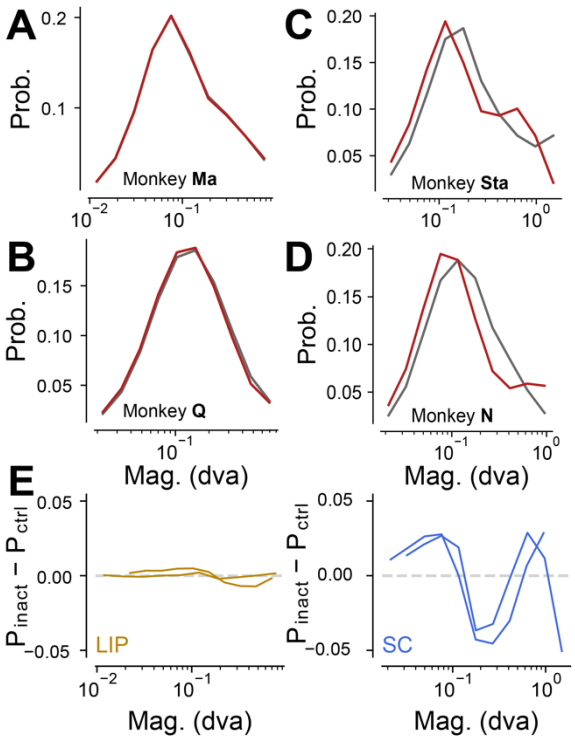

Figure S5: Eye movements within fixation during muscimol inactivation of LIP and SC. A-B. Probability distribution of displacements between eye records at each successive 50ms sample during DMC trials' initial fixation period, control behavior (grey) vs. behavior during LIP inactivation (red). **C-D**. Same, but for SC inactivation experiments. **E**. Difference between probability distributions (inactivation - control) for each animal. Left: animals in LIP inactivation experiments; right: animals in SC inactivation experiments. Larger deviations from 0 signal stronger impacts of inactivation on eye movement patterns.

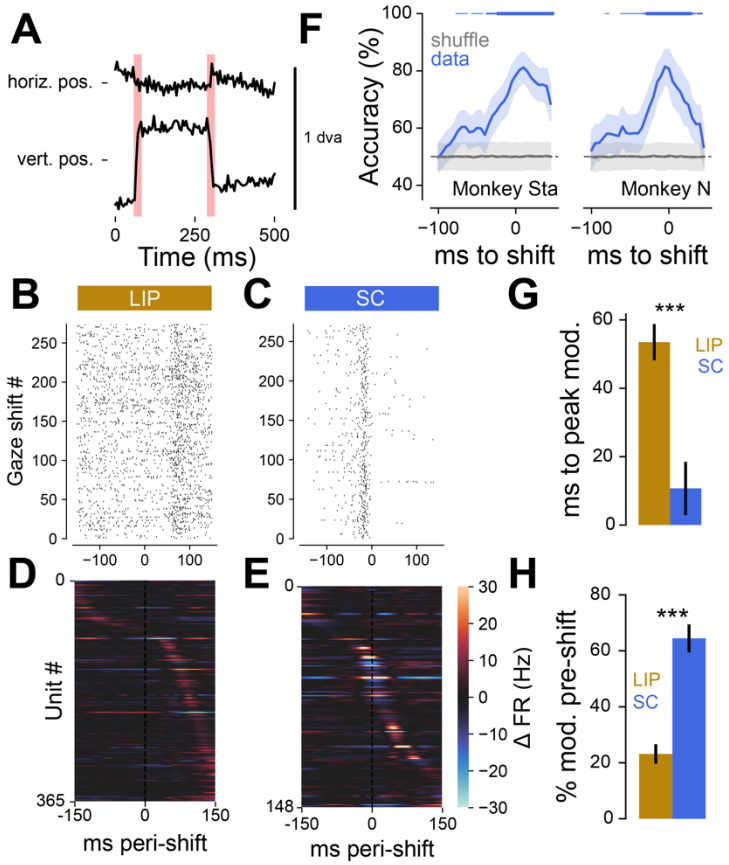

Figure S6: Neural activity in SC predicts upcoming miniature eye movements. **A**. Example gaze shift extraction from raw eye traces during the initial fixation period, one trial (Monkey Ho). **B**. Raster plot aligned to gaze shifts during the initial fixation period, 1 example LIP neuron. **C**. Raster plot aligned to gaze shifts during the initial fixation period, 1 example SC neuron. **D**. Heatmap of responses for all significantly gaze-shift-modulated units, LIP. **E**. Heatmap of responses for all significantly gaze-shift-modulated units, SC. **F**. Percent of shift-modulated units with significant modulation before shift onset (LIP and SC); error bars denote standard error of the mean proportion estimated via bootstrapping. **G**. Average latency to peak peri-shift response for all gaze-shift-modulated units, LIP and SC, mean +/- SEM (N = # modulated units). **H**. Decoding hemifield into which a gaze shift moves from pseudo-population activity in SC; left: Monkey Sta; right: Monkey N. Significant differences of decoding from chance (bootstrap test, FDR controlled via Benjamini-Hochberg procedure), shown in blue lines at top. Thickness of annotation bar denotes significance level (thinnest = $P < 0.05$, thickest = $P < 0.001$). Error bars denote standard error estimated via bootstrap. Classifiers trained and tested on activity at each timepoint.

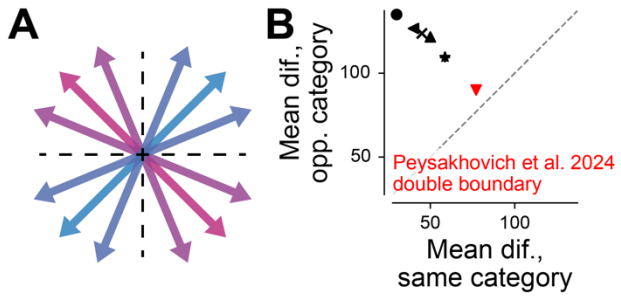

Figure S7: A double category boundary discourages similarity-based strategies during motion categorization tasks by increasing (decreasing) the average angular distance between pairs of directions in the same (opposite) category. **A**. Schematic of the double category boundary used in Ref.(5). Boundaries are shown in dotted black lines; each colored arrow represents 1 motion direction used in the experiment, colored by category assignment. **B**. Summary across DMC experiments of average distance between direction pairs belonging to the opposite vs. same categories; the distances for the double boundary are marked in red. The dotted line denotes unity – where the average angular distance is the same for direction pairs in the same and opposite categories. The ease of executing a similarity-based strategy decreases with increased proximity to this unity line.

Tables
Table S1: Task details

Dataset	Timings	Directions in C1	Directions in C2	Diameter, speed	Fixation window radius range
Freedman and Assad (2006), boundary 1	Fix: 500ms; Sample: 650ms; Delay: 1000ms; Test: 650ms	150, 180, 210, 240, 270, 300	330, 0, 30, 60, 90, 120	9 dva, 12 dva/s	1.5 dva
Freedman and Assad (2006), boundary 2	Fix: 500ms; Sample: 650ms; Delay: 1000ms; Test: 650ms	60, 90, 120, 150, 180, 210	240, 270, 300, 330, 0, 30	9 dva, 12 dva/s	1.5 dva
Fitzgerald, Freedman, and Assad (2011)	Fix: 500ms; Sample: 650ms; Delay: 1500ms; Test: 650ms	15, 255, 315	75, 135, 195	4-9 dva, 12 dva/s	1.4 - 1.75dva
Swaminathan and Freedman (2012)	Fix: 500ms; Sample: 650ms; Delay: 1000ms; Test: 650ms	75, 135, 195	255, 315, 15	9 dva, 12 dva/s	2 dva
Rishel, Huang, and Freedman (2013)	Fix: 500ms; Sample: 650ms; Delay: 1500ms; Test: 650ms	90, 180	270, 0	5 dva, 12 dva/s	2 dva - 3 dva
Sarma et al (2016)	Fix: 667ms; Sample: 667ms; Delay: 1013ms; Test: 667ms	67.5, 112.5, 157.5, 202.5	247.5, 292.5, 337.5, 22.5	9 dva, 12 dva/s	2 dva - 2.5 dva
Mohan et al (2021)	Fix: 500ms; Sample: 650ms; Delay: 1000ms; Test: 650ms	55, 75, 135, 195, 215	235, 255, 315, 15, 35	9 dva, 12 dva/s	2 dva
Zhou et al (2022)	Fix: 500ms; Sample: 650ms; Delay: 1000ms; Test: 650ms	55, 75, 135, 195, 215	235, 255, 315, 15, 35	9 dva, 12 dva/s	2.5 dva
Peysakhovich et al (2024)	Fix: 500ms; Sample: 550ms; Delay: 1200ms; Test: 550ms	112.5, 135, 157.5, 292.5, 315, 337.5	22.5, 45, 67.5, 202.5, 225, 247.5	6 dva, 10 dva/s	2.5 dva - 3.5 dva

Table S2: Dataset shape information

Animal	Experiment	Brain area	# sessions	# neurons
Monkey Ho	Freedman & Assad (2006), boundary 1	LIP	38	34
Monkey Ho	Freedman & Assad (2006), boundary 1	MT	27	23
Monkey Ho	Freedman & Assad (2006), boundary 2	LIP	21	19
Monkey Sti	Freedman & Assad (2006), boundary 1	LIP	49	44
Monkey Sti	Freedman & Assad (2006), boundary 1	MT	40	40
Monkey Sti	Freedman & Assad (2006), boundary 2	LIP	43	41
Monkey Ho	Fitzgerald et al. (2011)	LIP	58	55
Monkey I	Fitzgerald et al. (2011)	LIP	33	32
Monkey J	Swaminathan & Freedman (2012)	LIP	30	40
Monkey J	Swaminathan & Freedman (2012)	PFC	50	238
Monkey J	Swaminathan & Freedman (2012)	Area 5	29	47
Monkey B	Swaminathan & Freedman (2012)	LIP	22	27
Monkey B	Swaminathan & Freedman (2012)	PFC	40	210
Monkey B	Swaminathan & Freedman (2012)	Area 5	34	49
Monkey J	Rishel et al. (2013)	LIP	39	39
Monkey Ma	Rishel et al. (2013)	LIP	31	31
Monkey He	Sarma et al. (2016)	LIP	50	124
Monkey D	Sarma et al. (2016)	LIP	59	146
Monkey B	Mohan et al. (2021)	LIP	46	45
Monkey Ma	Mohan et al. (2021)	LIP	55	63
Monkey Q	Zhou et al. (2022)	LIP	24	138
Monkey Q	Zhou et al. (2022)	MST	43	359
Monkey Ma	Zhou et al. (2022)	LIP	21	29
Monkey Ma	Zhou et al. (2022)	MST	94	135
Monkey Sta	Peysakhovich et al. (2024)	LIP	13	331
Monkey Sta	Peysakhovich et al. (2024)	SC	12	244
Monkey N	Peysakhovich et al. (2024)	LIP	36	232
Monkey N	Peysakhovich et al. (2024)	SC	26	367